Carbon 177 (2021) 366–376

Contents lists available at ScienceDirect

Carbon

journal homepage: www.elsevier.com/locate/carbon

Research Article

Temperature dependent Raman scattering of directly grown twisted bilayer graphene films using low pressure chemical vapor deposition

Girija Shankar Papanai [a, c], Jasveer Singh [b], Nita Dilawar Sharma [b, c], S.G. Ansari [d], Bipin Kumar Gupta [a, c, *]

[a] Photonic Materials Metrology Sub Division, Advanced Materials and Device Metrology Division, CSIR-National Physical Laboratory, Dr. K. S. Krishnan Marg, New Delhi, 110012, India
[b] Pressure, Vacuum and Ultrasonic Metrology Section, Physico Mechanical Division, CSIR-National Physical Laboratory, Dr. K. S. Krishnan Marg, New Delhi, 110012, India
[c] Academy of Scientific and Innovative Research (AcSIR), Ghaziabad, 201002, India
[d] Centre for Interdisciplinary Research in Basic Sciences, Jamia Millia Islamia, Jamia Nagar, New Delhi, 110025, India

ARTICLE INFO

Article history:
Received 9 November 2020
Received in revised form
15 February 2021
Accepted 15 February 2021
Available online 26 February 2021

ABSTRACT

To get insight into the thermal management of twisted bilayer graphene based devices, the interpretation of temperature variation on twisting properties becomes crucial. In this aspect, we report the temperature dependent Raman scattering of twisted bilayer graphene (tBLG) on the Si substrate having SiO_2 thickness 300 nm. The tBLG samples have been directly grown on the copper foil substrate using a home-built low pressure chemical vapor deposition (LPCVD) setup. The temperature dependent Raman scattering has been studied on two samples of tBLG named as tB_1 and tB_2. The twisting nature of bilayer graphene film has been analyzed using R, G, and 2D peak characteristics in Raman spectra. The Raman mapping with respect to different peak parameters of G and 2D peak (intensity, width, and position), intensity ratio (I_{2D}/I_G) has been employed to probe the uniformity of tBLG film. In tB_1, the R peak has been found at 1395.82 cm^{-1} and not observed in sample tB_2 at room temperature. The temperature dependence of G and 2D peak frequency in Raman spectra has been investigated in the temperature range from 80 to 450 K. In tB_1 and tB_2, the temperature coefficient of G peak has been found to be - $(0.97 \pm 0.34) \times 10^{-2}$ cm^{-1}/K, and - $(1.08 \pm 0.15) \times 10^{-2}$ cm^{-1}/K, respectively. Further, the extracted value of temperature coefficient of 2D peak in tB_1, and tB_2 are - $(2.92 \pm 0.80) \times 10^{-2}$ cm^{-1}/K, and - $(3.01 \pm 0.29) \times 10^{-2}$ cm^{-1}/K respectively. Additionally, the twist angle has been estimated as ~23°-27° for $T \leq 300$ K and 3°-8° for $T > 300$ K in tB_1. In tB_2, it has been found to be ~13°-16° for the temperature range of 80–200 K and 5°-9° for 250–450 K. These findings shed light on the twisting behavior of bilayer graphene film and its anharmonic properties.

1. Introduction

The remarkable optical and electronic properties of the twisted bilayer graphene (tBLG) make it an attractive and potential candidate for the global physics communities in recent years [1–3]. It has drawn considerable theoretical and experimental attention because of the fascinating feasibilities to control the electronic structure by the random rotational configurations [4–6]. This purely carbon-based material exhibits exotic phenomena such as unconventional superconductivity, anomalous Hall effect, correlated insulating phases, and band topology [7–9]. The twisted or misoriented bilayer graphene forms, when the top or bottom atomic planes are rotated by an arbitrary angle (θ) about the perpendicular axis of the graphene surface. A superlattice structure has been generated with a larger unit cell than the single atomic plane, and create a Moiré pattern, which induces a periodic potential [10,11]. The AB stacked graphene (Bernal stacking) is the most stable form in which the layers are at $\theta = 0°$, and 60° that corresponds to metastable configuration referred to as AA stacked graphene. This new degree of freedom (θ) can be categorized in the two different regimes: small twist angle and large twist angle. In

* Corresponding author. Photonic Materials Metrology Sub Division, Advanced Materials and Device Metrology Division, CSIR-National Physical Laboratory, Dr. K. S. Krishnan Marg, New Delhi, 110012, India.
E-mail addresses: bipinbhu@yahoo.com, guptabgupta@nplindia.org (B.K. Gupta).

https://doi.org/10.1016/j.carbon.2021.02.083
0008-6223/

the first case, the layers are strongly hybridized due to strong interlayer interaction, and in the second one, the layers are strongly decoupled due to the small interlayer interaction. The twisting between layers induces several properties, namely Brillouin zone reshaping in a periodic structure, symmetry breaking in non-periodic structure, and tuning the optical properties [12]. The superlattices can give rise to flat bands near the Fermi level in the electronic structure and the low energy van Hove singularity in the density of states [13–15]. These dispersion less bands propounded that the twist angle variation can affect the nature of the electron from ballistic to localized in bilayer graphene. There are several methods to prepare the tBLG, namely mechanical exfoliation, using AFM tip, controlled flux of water, chemical vapor deposition, and precipitation from SiC [2,16]. The tBLG appears naturally in the graphene system, generally at the surface of crystalline graphite and during the CVD synthesis of bilayer graphene [17–19]. However, the other methods are complicated, probabilistic, and produce low yield except for the CVD method.

Therefore CVD method is highly preferred to grow the continuous, large scale and high-quality film. Kim et al. had artificially grown tBLG by superimposing the two CVD graphene layers [20]. Recently Chen et al. synthesized the mm-sized tBLG using a plasma-enhanced CVD method in which the twist angle can be controlled up to 20° [21]. Traditionally, the CVD grown graphene layers-have the most probability to reveal the Moiré pattern for a range of twist angles. Various characterization techniques such as optical microscopy, atomic force microscopy (AFM), Raman spectroscopy, infrared spectroscopy, high-resolution transmission electron microscopy (HRTEM), scanning tunneling microscopy (STM), and Landau level spectroscopy have been used to study the properties of twisted bilayer graphene [2,22,23]. Among these, Raman spectroscopy is one of the rapid, most informative, facile, non-dissipative, and non- destructive successful technique to characterize the carbon-based materials and provide structural as well as electronic information with high resolution. The optical, electronic, and phonon properties are easily determined based on Raman spectral features such as intensity, peak position, peak width, and peak shape of G and 2D modes, respectively [24]. In tBLG, significant changes have been observed in the Raman spectra through the resonance enhancement and superlattice induced Raman scattering as a function of twist angle [20,25,26].

On the other hand, the temperature dependent Raman study becomes essential to understand the thermal properties and convenient to establish the metrology in graphene at the nanoscale [27,28]. It has been observed that the high current annealing can remove the contaminants from the graphene surface and become useful to obtain clean graphene devices [29]. During the transport measurement, a self-heating effect arises due to current conduction between source and gate terminals of FET as well as the appearance of thermal resistance on the interfaces of different materials. These observations manifest that the graphene is sensitive to the ambient temperature. In tBLG, the van der Waals interaction between the layers hinders the propagation of electron and phonons, which makes the thermal conductivity lower as compared to single layer graphene (SLG) and AB stacked bilayer graphene [30]. Calizo et al. have studied the temperature dependent Raman spectra and obtained the G peak temperature coefficient of −0.0162 and −0.0154 cm^{-1}/K of SLG and bilayer graphene, respectively in the temperature range 83–373 K for the first time [31]. Zhou et al. have reported the Raman spectra of SLG in the temperature range of 303–473 K [32]. Wang et al. have studied that temperature dependent Raman spectra of SLG synthesized by the CVD method on copper foil substrate and the temperature coefficients of G and 2D peak are extracted to be −0.101 and −0.180 cm^{-1}/K in the temperature range of 150–390 K respectively [33]. Keeping these aspects in view, here we present the temperature dependent Raman spectroscopy of twisted bilayer graphene films, which is grown by low pressure chemical vapor deposition method. To the best of our knowledge, the variation of twisting nature with temperature has not been reported so far.

2. Materials and methods

2.1. Synthesis of twisted bilayer graphene film

Various samples of tBLG film have been synthesized using 25 μm thick polycrystalline copper foil (Alfa Aesar, purity 99.999%) as a substrate. Prior to growth, the copper has been cleaned with acetone, deionized (DI) water, acetic acid, and IPA, successively. The home built LPCVD setup has been used to synthesize the bilayer graphene film and directly grown over the copper foil. Previously, this setup has been used to grow the high-quality SLG by our research group [34]. The different samples have been grown by varying the annealing time of copper from 30 to 50 min. The growth conditions of the two best samples (tB_1 and tB_2) are the following-

Sample tB_1

Initially, the pretreated copper foil is placed on the quartz plate and loaded in the isothermal zone of the reaction chamber. After evacuating, the mixture of Ar and H_2 gas with partial pressure ratio ($P_{H_2} : P_{Ar} = 1 : 1$) has been introduced in the reaction chamber, at a pressure of 11.2 ± 0.4 Torr. The desired pressure has been controlled by a mass flow meter, rotameter, and a valve between the quartz tube outlet and a rotary pump. The annealing has been performed in the presence of a mixture of Ar and H_2 gas for 30 min at 1000 °C. After annealing, the Ar gas has been turned off and pressure adjusted to 14.5 ± 0.5 Torr using the flow of H_2 gas before introducing the methane gas. The partial pressure ratio ($P_{H_2} : P_{CH_4} = 2 : 1$) has been maintained at a pressure of 17 ± 0.3 Torr after introducing the methane (CH_4) gas in the chamber, and the growth has been carried out for 3 min at 1000 °C. After growth, cooling has been started by opening the furnace and continued up to 100 °C in the presence of a mixture of H_2 and Ar gas flow at the initial pressure. The sample has been taken out after completion of the growth process.

Sample tB_2

In the synthesis of tB_2, the copper foil has been annealed for 50 min at 1000 °C in the presence of a mixture of Ar and H_2 gas. Other growth parameters are maintained as similar to tB_1.

2.2. Transfer of twisted bilayer graphene film from copper foil to Si/SiO_2 substrate

The wet chemical method has been used to transfer the tBLG film with the assistance of PMMA mediated approach. PMMA has been spin-coated on tBLG/Cu stack for 1 min at 4000 rpm using a solution of 4% PMMA (495 kg/mol) in anisole. The copper has been etched via dissolving the PMMA/tBLG/Cu stack in an etching solution comprising 20% of $(NH_4)_2S_2O_8$ in DI water. The modified RCA cleaning method has been used for the cleaning of the PMMA/tBLG stack and transferring the tBLG over Si/SiO_2 substrate [35].

2.3. Optical microscopy

The optical microscopy technique has been used to visualize the synthesized tBG film over the copper foil and Si substrate having SiO_2 thickness 300 nm (GMS-India). The DSX1000 digital microscope has been used in the bright field mode with the objective lens DS×10-XLOB20X having NA and working distance 0.4 and 20 mm, respectively.

2.4. Raman Spectroscopy

Raman Spectroscopy has been carried out by Triple JobinYvonT64000 Raman Spectrometer. The Ar ion laser with an excitation wavelength of 514.5 nm was focused on the sample by a 20× objective. For the temperature dependent Raman spectroscopy measurements, all the samples with dimension 2 mm × 2 mm have been placed in the sample holder in a cryostat and the chamber is evacuated up to a base pressure of 10^{-6} Torr via turbomolecular pump. The temperature controller has been used to achieve the temperature of 80 K with the help of liquid nitrogen (LN_2), and high temperature (450 K) can be attained using a temperature controller (Lake Shore Cryotronics-335). The laser spot position was fixed at the center of the sample throughout the measurement. Initially, the sample has been cooled from room temperature (300 K) to low temperature (80 K), and then 80 K onwards, the Raman spectra are collected. Afterward, the Raman spectra have been captured from 80 K to 450 K and then return to 300 K. We waited about 20–25 min for temperature stability on the sample stage after reaching the desired temperature. Raman mapping has been performed by the laser source Renishaw inVia Raman microscope, having 532 nm excitation wavelength with 20 × magnification, and 2400 l/mm grating under laser power of 5 mW. Although two excitation wavelength, 514.5 and 532 nm have been used during the experiment, the conclusion has been made based on the 514.5 nm. The temperature dependent facility was not available with the Renishaw inVia Raman microscope.

3. Results and discussion

3.1. Optical microscopy of tBLG film over Cu foil and Si/SiO_2 substrate

The LPCVD method has been used to synthesize the twisted bilayer graphene film. The optical images of two samples (tB_1, and tB_2) which are primarily grown on the copper foil and is shown in Fig. S1. One can observe the Cu grains and grain boundaries, which are clearly visible in tB_1 and tB_2. The variation in annealing time significantly changes the Cu grain size, and it varies due to recrystallization and reorientation of polycrystalline Cu. The Cu grain size has been measured from different locations of optical images and found up to ~1.2 mm approximately. In earlier studies, it has been shown that the graphene quality can be improved by minimizing the Cu grain boundaries, which enlarge the grain size of Cu and hence increases the grain size of graphene [36]. Fig. 1a and b shows the optical images of tB_1, and tB_2, after transfer over Si/SiO_2 substrate, and the inset shows the lateral view of the graphene/SiO_2 stack. The optical image represents the continuous film of graphene in which significantly less amount of PMMA residues and cracks are present. It manifest that the prepared graphene is very less damaged during the etching and transfer process. The optical images have been captured at different times in different optical settings; therefore, the contrast variation appears in Fig. 1.

3.2. Raman Spectroscopy of tBLG films and twist angle estimation at room temperature

For Raman studies, the samples are transferred from Cu foil to Si/SiO_2 substrate, and this spectroscopic technique has been used to probe the quality, the number of atomic planes, stacking order, and orientation between two graphene layers in different samples [24]. Fig. 2 shows the variation of different peaks in the Raman spectra of tB_1 and tB_2 at room temperature in the rectangular region of Fig. 1. The position, width, and intensity of the most notable peaks, namely D, G, and 2D, have been listed in Table 1, which plays a vital role in perceiving the nature of the samples. All the peak parameters are obtained using the Lorentzian fitting. It has been noticed that the G and 2D peak intensity decreases, and the I_D/I_G ratio increases as move from tB_1 to tB_2 (see Table 1 for values). The measurement of the disorder has been analyzed by the intensity of D band and gives information about the crystallinity and quality of samples.

The D peak is ascribed to breathing modes of six atom rings and associated with the one defect and one in-plane transverse optical phonon [37]. On the basis of intensity ratio (I_D/I_G), it has been seen that tB_1 is less defective as compared to other samples.

However, the number of layers has been identified based on the combination of two parameters: 2D peak width and peak intensity ratio (I_{2D}/I_G) [24]. The G peak originated from the first-order scattering process, which is directly related to doubly degenerate in-plane transverse optical (iTO) and longitudinal optical (LO) phonon modes at the Brillouin zone center [38]. The 2D peak arises due to two in-plane transverse optical phonons near the K point [39]. In tB_1, the 2D peak shows more intensity than the G peak having 2D to G ratio ~1.08. Similarly, in tB_2, the 2D peak shows a higher intensity than the G peak with 2D to G ratio ~1.91. On the basis of intensity ratio (I_{2D}/I_G), both samples indicate that the bilayer graphene has been formed. In previous reports, the intensity ratio (I_{2D}/I_G) and 2D peak width have been found to be ~ $1 \leq I_{2D}/I_G < 2$ and 45-60 cm^{-1} in AB stacked bilayer graphene [40,41]. However, the 2D peak width has been found smaller as compared to the AB stacked bilayer graphene in both samples, and it clearly indicates that the prepared bilayer graphene film has the presence of twisting between the layers. Further, the Raman spectra have been captured under the excitation wavelength of 532 nm at the random locations of the tB_1 and tB_2 to probe the nature of twisting in the bilayer graphene (Fig. S2). In both the samples, the properties of G and 2D peaks, such as peak width and intensity ratio (I_{2D}/I_G), have been evaluated from the Raman spectra (Table S1). Table S1 reveals that most of the regions (marked by numbers in the optical image) have the presence of twisting in the bilayer graphene.

Furthermore, Raman mapping has been performed to probe the uniformity of the different vibrational modes in both the samples before temperature dependent measurements. The Raman mapping has been employed at the rectangular region of Fig. 1 having an area of 20 μm × 18 μm. Fig. 3 shows the Raman mapping with respect to peak intensity, peak width, and peak position of G and 2D modes, intensity ratio (I_{2D}/I_G) in tB_1 and tB_2. The intensity map of G and the 2D peak of tB_1 and tB_2 have been shown in Fig. 3a and b, and Fig. 3g and h. The color contrast of intensity images clearly shows that the 2D peak has more intensity as compared to G peak in most regions of tB_1 and tB_2. The peak width of G and the 2D peak of tB_1 and tB_2 has been shown in Fig. 3c and d, and Fig. 3i and j. The color contrast of the peak width map also shows the small variation in G and 2D peak throughout the mapped region. The peak position of G and the 2D peak of tB_1 and tB_2 have been demonstrated in Fig. 3e and f, and Fig. 3k and l. The peak position map of G and 2D peak shows that tB_2 is more uniform as compared to the tB_1. However, the 2D peak width map of both samples in some regions shows the features of SLG and AB stacked bilayer graphene. This property indicates that large and small twist angles are present in the mapped region of samples. The intensity ratio (I_{2D}/I_G) mapping in sample tB_1 and tB_2 has been demonstrated in Fig. 3m, n. The color contrast illustrates that I_{2D}/I_G variation is smaller in tB_1 as compared to tB_2. The higher value of I_{2D}/I_G in tB_1 indicates the presence of large twist angle in most of the regions. In the case of tB_2, color contrast reveals that both small and large twist angles exist in the mapped region.

To ensure the reproducibility of the presence of twisting, the various samples of the tBG film have been prepared and one of the

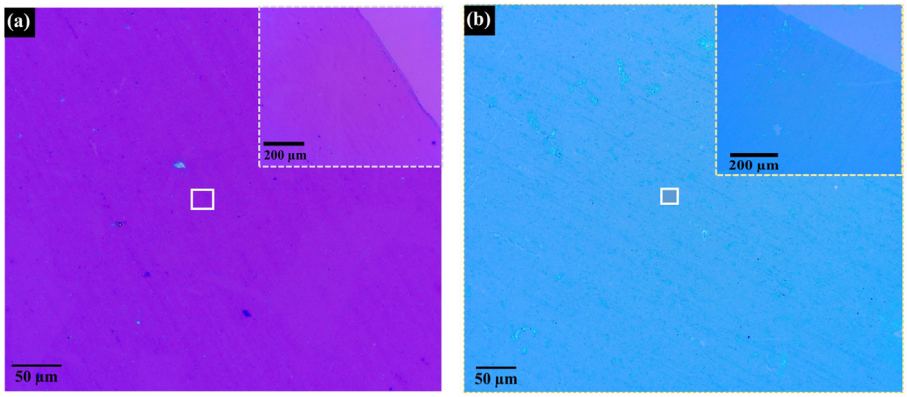

Fig. 1. The optical microscopy images of twisted bilayer graphene film over Si substrate having SiO_2 thickness 300 nm with scale bar 50 μm: (a) Sample tB_1. (b) Sample tB_2. The inset displays the lateral view of the tBLG/Si stack in each sample with a scale bar of 200 μm.

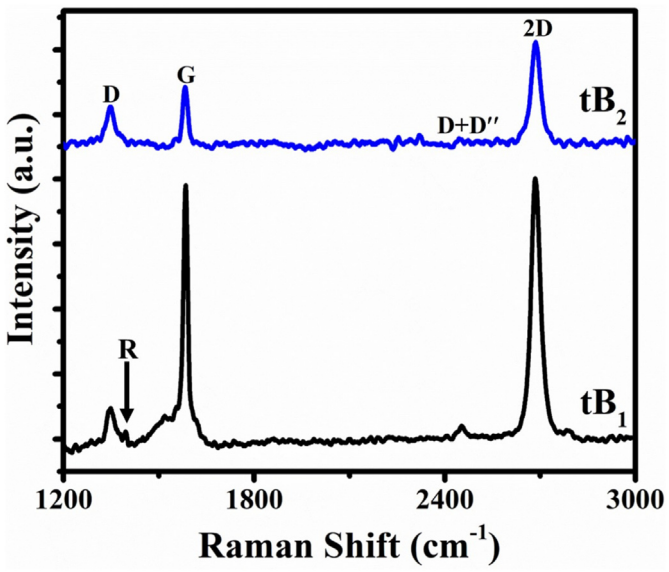

Fig. 2. Raman spectra of sample tB_1 and tB_2 on the Si/SiO_2 substrate with an excitation wavelength of 514.5 nm at room temperature and captured inside the rectangular region of optical images.

sample has been shown in Fig. S3. The Raman characteristics at the random locations of the optical image shows the similar spectral properties and proves the presence of twisting (Fig. S3). The Raman mapping with respect to peak intensity, peak width, and peak position of G and 2D peak displays that most of the region is the twisted bilayer region (Fig. S3). The presence of twisting directly affects the phonon band structure by virtue of the modification in the Brillouin zone size and interlayer interaction [42]. In previous reports, it has also been noticed that some Raman modes are very sensitive to the number of atomic planes and interlayer coupling, which are directly related to the stacking order [43,44]. These double resonant peaks are known as R and R′ in the Raman spectra of twisted bilayer graphene and originated due to twist angle between the layers [25,45,46]. The R peak is ascribed to the intervalley process and came from the transverse optical (TO) phonon branch, and the R′ peak originated from the intravalley double resonance process (LO phonon) in which Umklapp scattering occurs through the superlattice potential [25].

In particular, the R and R′ peaks are non-dispersive in nature because the energy of phonons is uniquely determined by the twisting wave vector. The appearance of both peaks is not related to the presence of disorder, and the momentum conservation is mediated by the superlattice wave vector in place of defects. In addition, the twisting modified the band structure through the Dirac cones overlapping in the top and bottom layers of graphene. The strong interaction in the overlapping region induces the Van Hove singularity in the density of states, and it is directly affected by the position of the overlapping region due to variation in twist angle [47]. The twist angle, at which the energy difference between the Van Hove singularities of conduction and valence band matches with the laser excitation energy, which we will refer to as the resonant critical angle (θ_c). Moreover, several changes have been noted in Raman spectra close to θ_c in which G peak intensity enhancement is one of them, and also, the 2D peak width becomes close to SLG at the large angles and has a considerable value at a small twist angle in previous studies [20,47]. Therefore, the above-mentioned factors are taken into consideration to estimate the twist angle from the Raman spectra in all the samples. The resonant critical angle can be determined by the Dirac dispersion relation of SLG and expressed as [20]-

$$\theta_c = \frac{\Delta k}{K} = \frac{3aE_{laser}}{2h\nu_f} \quad (1)$$

where a is the lattice parameter (a = 0.246 nm), v_f is the Fermi velocity in SLG (10^6 m/s), E_{laser} is the excitation energy, and h is the

Table 1
The peak position, peak intensity, peak width of D, G, and 2D peaks along with the intensity ratios (I_{2D}/I_G, I_D/I_G) of samples tB_1 and tB_2 at 300 K.

Samples	Peak Position (cm^{-1})			Peak Intensity (a.u.)			Peak Width (cm^{-1})			Intensity Ratio	Intensity Ratio
	D	G	2D	D	G	2D	D	G	2D	I_{2D}/I_G	I_D/I_G
tB_1	1347.62	1584.44	2686.05	22.90	199.45	214.68	25.37	14.91	34.17	1.08	0.11
tB_2	1347.07	1583.39	2686.25	25.93	42.30	80.88	27.53	18.08	35.01	1.91	0.61

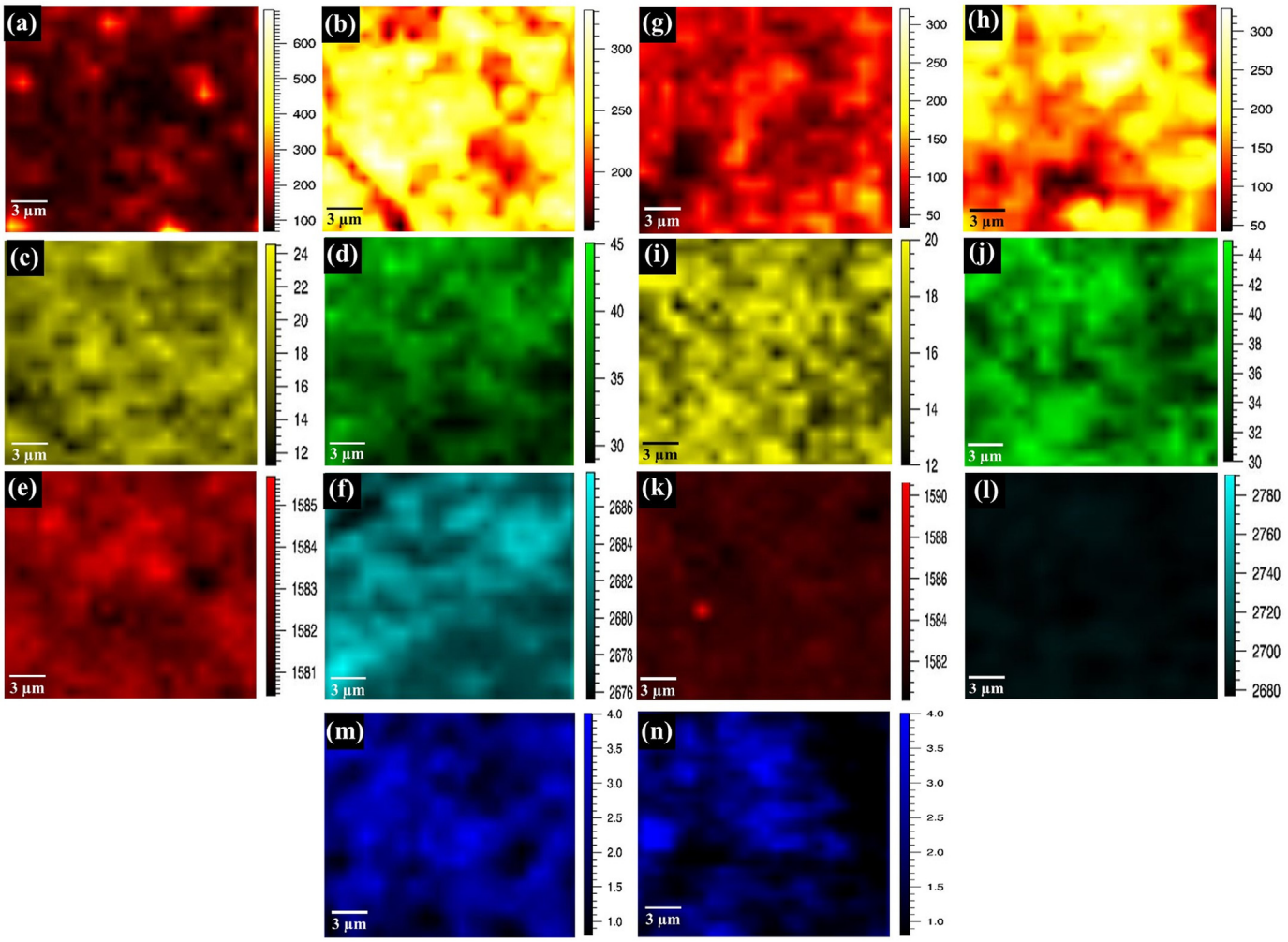

Fig. 3. The Raman mapping of twisted bilayer graphene film in the rectangular region of optical images: (a–f) Mapping with respect to (a,b) intensity, (c,d) peak width, and (e,f) peak position of G and 2D peak in sample tB_1. (g–l) Mapping with respect to (g,h) intensity, (i,j) peak width, and (k,l) peak position of G and 2D peak in sample tB_2. Intensity ratio (I_{2D}/I_G) mapping: (m) in sample tB_1, (n) in sample tB_2. All the Raman images having a scale bar of 3 μm.

Planck constant. The resonant critical angle (θ_c) has been found to be ~ 12° for the laser excitation of 514.5 nm. In order to estimate the twist angle, the R, G, and 2D peak parameters have been obtained from the Raman spectra. In the previously published literature, the twist angle has been assigned uniquely on the basis of 2D and G peak parameters (position, intensity, and width) along with R and R′ peak position also [20,25,47,48]. In tB_1, the R peak shows the peak position 1395.82 cm^{-1} , which can be seen from Fig. 2. The twist angle was found to be ~24° and was estimated by the R peak position from earlier reports [48,49]. In tB_2, no R peak has been observed in the Raman spectra at the 300 K. In this context, the 2D and G peak information becomes valuable for identifying the twist angle. The twist angle has been estimated ~ 8° in tB_2 based on the earlier reports [20,47,50]. The estimated twist angle in both samples is not close to θ_c and the significant difference in Raman spectra may be believed as the Dirac cones proximity via the strong coupling between layers in momentum space for $\theta < \theta c$ and the occurrence of optical transition in isolated Dirac cones for $\theta > \theta c$ [20]. For further confirmation of twisting nature, the 2D peak shape has been analyzed using deconvolution. Generally, the 2D peak shows a single Lorentzian feature having a peak width of 24 cm^{-1} in SLG. The same peak width has been considered to define a characteristic lifetime for the double resonance process [38]. Therefore, we fitted the 2D peak by fixing the peak width at 24 cm^{-1} in all cases. The 2D peak spectra with their corresponding Lorentzian components are vertically stacked for clarity (Fig. S4). In both samples, the 2D peak was fitted using three Lorentzian components, all of them having the same peak width of 24 $cm^{-1,}$ but their peak position and peak intensity are different. Generally, it has been observed that the 2D peak consists of four Lorentzian components in AB stacked bilayer graphene [24]. The reduction of four components into three components attributed to the symmetric nature of valence and conduction band in bilayer graphene [38]. Both samples can be easily distinguished from the comprising 2D peak components (Fig. S4). Carozo et al. have shown that the 2D peak composed of multiple peaks for $\theta \leq 7°$ and single Lorentzian having a peak width of 23 cm^{-1} in the case of $\theta > 7°$ [48]. But in the present study, a 2D peak is composed of multiple (three) peaks in all the samples for small as well as the large twist angle at 300 K.

3.3. Temperature dependent Raman spectroscopy of sample tB_1

The Raman spectra of sample tB_1 in the temperature range 80–450 K are shown in Fig. 4. The temperature variation directly affects the peak features in the Raman spectra, which can be observed from Fig. 4. Further, the temperature dependence of G and

2D peak position of sample tB_1 has been shown in Fig. 5a and b. The G and 2D peak positions are red-shifted as the temperature increases, and their frequency shifts are found to be 5.43 and 14.14 cm^{-1}, respectively.

The temperature variation in phonon frequency as a result of anharmonic lattice vibrations and the peak frequency of G and the 2D peak has been described by the following equation

$$\omega^{G,2D} = \omega_0^{G,2D} + \chi^{G,2D}T \quad (2)$$

where $\omega_0^{G,2D}$ is the peak frequency of G and 2D peak when the temperature (T) is extrapolated to 0 K, and $\chi^{G,2D}$ is the first-order temperature coefficient of G and 2D peak.

The experimental range of temperature (80–450 K) is less than the Debye temperature of the graphite layer (~2500 K); therefore, the higher-order terms in Equation (2) do not appear. The $\chi^{G,2D}$ defines the slope and has been extracted from the fitted straight lines in Fig. 5a, and b. The temperature coefficient of G and 2D peak has been found - $(0.97 \pm 0.34) \times 10^{-2}$ cm^{-1}/K and - $(2.92 \pm 0.80) \times 10^{-2}$ cm^{-1}/K respectively. Nevertheless, the G peak shows a slight deviation from linear behavior in some of the data points. This data scattering may be ascribed to the sensitivity of G peak to the presence of defects, drift in laser spot during the transition among required temperatures, and variation in the laser power on the sample during the cooling and heating process. The extrapolated peak frequency of G and 2D peak at 0 K has been found 1586.37 and 2691.99 cm^{-1}, respectively. The higher value of temperature coefficient of the 2D peak as compared to G peak may be due to second order phonon process and also the effect of thermal expansion on C–C bonds. In the past, several authors have studied the temperature coefficient of carbon-based materials and noticed that two factors contribute mainly to the temperature coefficient, one is self-energy, and the other is the thermal expansion [31,51]. Also, the thermal expansion coefficient (TEC) mismatch between graphene and substrate may also affect the experimental data due to the temperature variation [52]. Further, the temperature dependence of the peak width along with the peak area and intensity ratio of G and the 2D peak has been shown in Fig. S5. The G and 2D peak width was found in the range of 14.91–21.06 cm^{-1} and 32.95–49.52 cm^{-1}; the intensity ratio (peak height, I_{2D}/I_G) and intensity ratio (peak area, A_{2D}/A_G) have been found in the range of 0.85–1.25 and 1.98–2.99, respectively (Fig. S5).

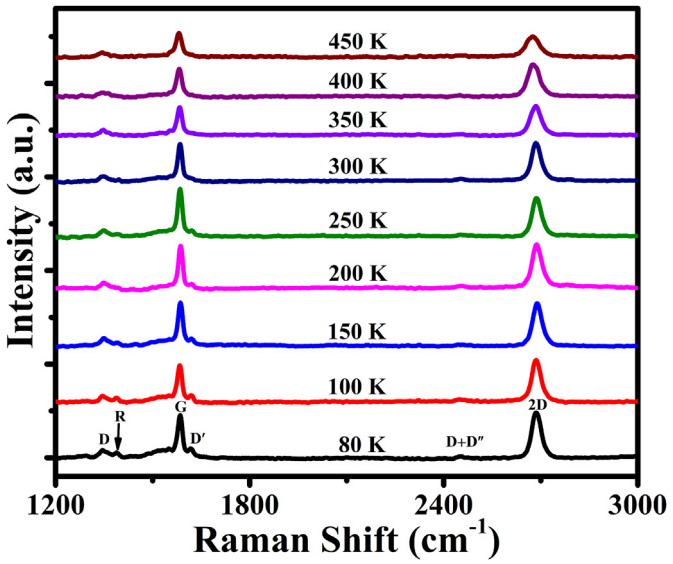

Fig. 4. Temperature dependent Raman spectroscopy of sample tB_1 over Si/SiO_2 substrate in the temperature range of 80–450 K. The obtained peaks are marked in Raman spectra at their respective positions.

Additionally, the 2D peak shape has been examined in the temperature range of 80–450 K (Fig. S6). It has been observed that the Raman spectra up to 350 K comprise of three Lorentzian components, and it consists of four Lorentzian in the case of 400 and 450 K (Fig. S6). The fitted parameters, such as peak position, peak width, and peak intensity, have been tabulated in Table S2. The number of comprising components are directly related to the splitting of electronic and phonon branches. Generally, the four optical processes are involved in the 2D peak, which corresponds to four components, and the appearance of three comprising Lorentzian for T < 400 K may be attributed to the presence of two degenerate processes in electron-phonon scattering [53]. Moreover, the Raman modes in the vicinity of the G peak are shown in Fig. 6, and for clarity, the temperature dependent Raman spectra are vertically stacked with different Y-axis offset values. It has been seen that the R peak disappears for the T > 300 K, and D' peak disappears for T > 250 K due to very low intensity as compared to D and G peak. The peak positions of D, R and D' peaks at different temperature has been tabulated in Table S3.

The frequency shift in D, R, and D' peaks has been found to be 6.10, 7.31, and 2.95 cm^{-1}, respectively. Generally, the D' peak has been found at ~1620 cm^{-1}, and the random distribution of impurities along with surface charges induces the G peak splitting: G peak and D' peak. The G peak splitting occurs as a result of the interaction between localized vibrations of impurities and phonon modes. The D' peak originated from intravalley phonon and defect scattering in which one defect and one in-plane transverse optical phonon with $q \neq 0$ are involve near the Γ point [54,55].

3.4. Temperature dependent Raman spectroscopy of sample tB_2

Fig. 7 illustrates the temperature dependent Raman spectra of tB_2. The temperature dependence of G and 2D peak positions have been shown in Fig. 8a and b. Both G and 2D peak frequencies are red-shifted as the temperature increases.

The frequency shift in G and the 2D peak has been found to be 3.75 cm^{-1} and 11.19 cm^{-1}, respectively. The G and 2D peak frequencies are following the linear relation with respect to the temperature, which can be observed from Fig. 8a and b. The temperature coefficient of G and the 2D peak has been found to be- $(1.08 \pm 0.15) \times 10^{-2}$ cm^{-1}/K and - $(3.01 \pm 0.29) \times 10^{-2}$ cm^{-1}/K, respectively. The extrapolated peak frequency of G and 2D peak at 0 K has been found to be 1587.40 cm^{-1} and 2695.07 cm^{-1}, respectively. Further, the temperature dependence of peak width along with the peak area and intensity ratio of G and 2D peak, is depicted in Fig. S7.

The peak width of G and the 2D peak has been found in the range 17.38–18.86 cm^{-1} and 29.49–38.94 cm^{-1}, respectively (Fig. S7). On the other hand, the intensity ratios I_{2D}/I_G and A_{2D}/A_G have been obtained in the range of 1.54–2.73 and 2.96–4.91, respectively. Furthermore, the temperature dependence of the 2D peak has been shown in Fig. S8. It has been observed that the 2D peak consists of two and three Lorentzian having peak width 24 cm^{-1} for the temperature range 80–200 K and 250–450 K (Fig. S8). The two comprising components up to the temperature of 200 K indicate that the Raman spectra are similar to the SLG. The peak fitting details with the temperature variation have been tabulated in Table S4. In addition, the frequency shift has been found in D peak 9.14 cm^{-1} and no R, D' peaks have been found in the temperature range 80–450 K. Moreover, the temperature dependent Raman spectra of another sample have been shown in Fig. S9. The frequency shift in G and the 2D peak has been found to be 3.28 cm^{-1} and 14.15 cm^{-1}, respectively. Additionally, the

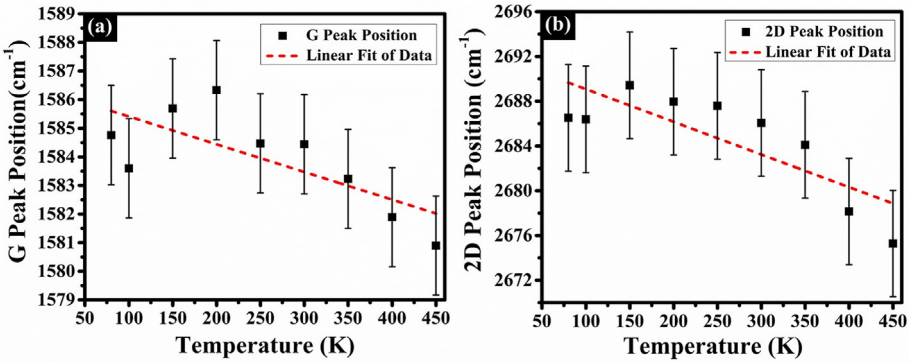

Fig. 5. The peak frequencies variation with respect to temperature in sample tB_1 from 80 to 450 K: (a) G peak frequency. (b) 2D peak frequency. The temperature coefficient ($\chi^{G,2D}$) has been extracted using the measured data. The red dashed lines illustrate the linear fit, and error bars represent the one standard deviation of data points.

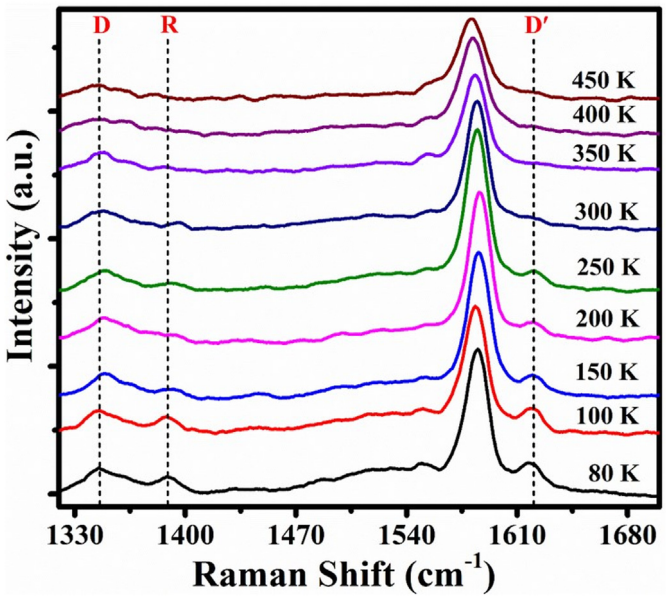

Fig. 6. The enlarged view of Raman spectra close to the G peak of sample tB_1 in the temperature range (80–450 K) and the peaks D, R, and D′ are represented by the dotted line.

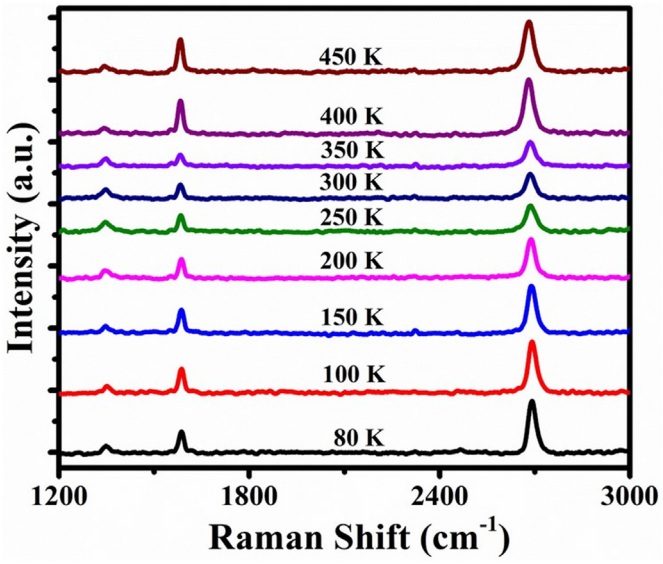

Fig. 7. Temperature dependent Raman spectroscopy of sample tB_2 over Si/SiO_2 substrate in the temperature range of 80–450 K.

temperature dependence of peak width along with the peak area and intensity ratio of G and 2D is shown in Fig. S10. The G and 2D peak widths have been found in the range 13.52–17.13 cm^{-1} and 30.76–38.92 $cm^{-1,}$ respectively (Fig. S10). In addition to this, the intensity ratios I_{2D}/I_G and A_{2D}/A_G have been found in the range of 0.69–1.04 and 1.47–2.47, respectively. Moreover, the 2D peak shape has been examined with temperature variation, as illustrated in Fig. S11. It is important to note that the 2D peak consists of two and three Lorentzian having peak width 24 cm^{-1} for a temperature of 80 K and 100–450 K (Fig. S11). Moreover, the R peak feature has been observed for temperature below 250 K, and the peak position has been found at 1395.69 and 1396.51 cm^{-1} for the temperature of 80 K and 250 K, respectively.

Next, we turn our attention towards the specific heat, which is one of the crucial parameters that directly probes the variation in thermal and phonon properties. The phonon density of states is required to know about phonon assisted processes, and the phonon energy affected by the interatomic potential strongly. Previously, the phonon specific heat in tBLG was calculated using Born-von-Karmann (BvK) model for intralayer interactions and spherical potential for interlayer interactions [56]. It was observed that the out-of-plane acoustic (ZA) phonons contributed most in specific heat for $T \leq 200$ K, and longitudinal acoustic (LA), transverse acoustic (TA), and ZA phonons contributed in the temperature range of 200–500 K. The significant changes have been observed in phonon specific heat at different twist angles below the temperature of 15 K and varied with $T^{1.3}$ [57]. At this temperature, twisting affects low-frequency ZA phonon modes strongly; however, considerable change has not been noticed in the phonon specific heat in the temperature range of 20–2000K. Nevertheless, we believe that the modification in phonon spectrum might affect the Raman spectra in the measured temperature range of 80–450 K in both the samples (tB_1 and tB_2).

Besides, in tB_1, and tB_2, it is worth noticing that the D + D′′ peak intensity varies with temperature, and it exhibits the weak feature when the peak intensity becomes comparable to the noise level. This peak has been found at ~2450 cm^{-1} and originated from a combination of phonon in a longitudinal acoustic (LA) branch and a D phonon [58]. Apart from this, a shoulder has been observed in the vicinity of G peak ~1550 cm^{-1} in tB_2. However, this peak shows a less pronounced feature and not found in tB_1. In previous reports, the G peak splitting in Raman spectra has been observed due to the

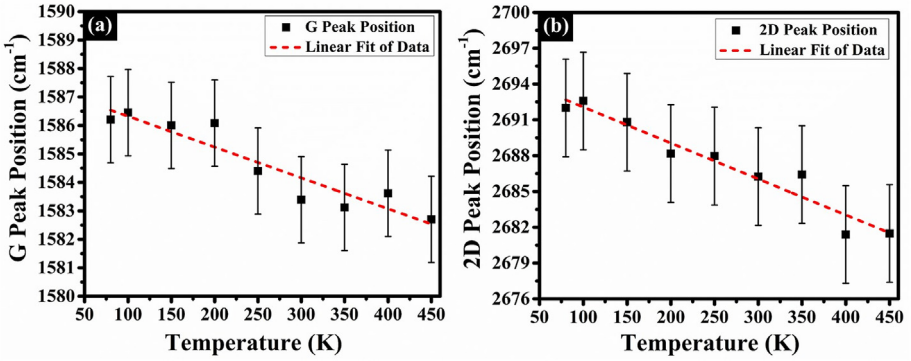

Fig. 8. The peak frequencies variation with respect to temperature in sample tB_2 from 80 to 450 K: (a) G peak frequency. (b) 2D peak frequency. The red dashed lines illustrate the linear fit, and error bars represent the one standard deviation of data points. (A colour version of this figure can be viewed online.)

presence of uniaxial strain and the effect of substrate on the graphene [59,60]. On the other hand, the molecular intercalation between two graphene layers and unintentional doping may cause the G peak splitting [61,62]. Although the shoulder is not extremely strong in comparison to the G peak, but the effect of strain and doping cannot be ignored.

3.5. Twist angle estimation in the temperature range of 80–450 K in samples tB_1 and tB_2

Prior to an estimation of twist angle, the understanding of different factors mainly doping, and graphene-substrate interaction, which affect the Raman measurement during temperature variation, is essential. Usually, the doping becomes strong when graphene is coupled tightly to the substrate and its exposure to oxygen, moisture. In the case of tBLG, the bottom layer is affected strongly due to its direct contact with the substrate compared to the top layer. When the temperature increases, the diatomic oxygen in SiO_2 might receive the charge from graphene. However, the doping effect in tBLG is not strong compared to SLG because fewer electrons are transferred to the top layer than the lower one, and the top layer is shielded from the substrate. In addition to this, the prepared tBLG has not been subjected to any air contamination deliberately, and the temperature dependent Raman measurement is carried out under a high vacuum. Therefore, we assume that the doping induces a negligible effect on the G and 2D peaks in Raman spectra.

Now, we discuss the strain generation by the underlying substrate due to the TEC mismatch between graphene and Si/SiO_2 substrate. In the past, several studies have seen the effect of Si/SiO_2 substrate on SLG along with the other substrates such as glass, copper, GaAs, sapphire also [33,52,63]. But in the case of tBLG, the presence of two layers creates a different situation from the SLG. In the course of heating (cooling) process, the bottom layer of graphene contracts (expands), and the SiO_2 layer expands (contracts). Due to this, the bottom layer experiences a compressive strain (cooling) or tensile strain (heating) during temperature variation. In this condition, the top layer has less influence on heating or cooling, which can be assumed as a strain-free layer. Although in a recent study, the asymmetric strain in isotopically labeled (^{12}C and ^{13}C) bilayer graphene over Si/SiO_2 substrate has been reported in different media under the pressure application [64], it has been noticed that a maximum of 0.1% strain difference is observed between the top and bottom layer under biaxial strain. However, the mechanical or chemical effects under the pressure variation are different from the temperature variation. In another study, Omambac et al. observed that the graphene on metallic substrate spontaneously reoriented due to biaxial pressure, which arises from the different thermal nature of graphene and substrate [65]. A commensurate-incommensurate phase transition occurs in bilayer graphene, when one layer experiences stretching or compression [66]. In both the conditions (heating or cooling), the elastic energy of the complete system (tBLG and Si/SiO_2 substrate) increases. Because of this, an incommensurability defect (ID) is formed, and a transition occurs from commensurate to incommensurate phase. This transition is previously explained on the basis of the modified Frenkel-Kontorova (FK) model, in which two harmonic chains of particles interact non-linearly, where one chain experiences strain, and the other is free [66]. The tBLG also exhibits the superlubric nature due to changes in the interlayer coupling [17,67]. The structural superlubricity varies with temperature, and superlubric sliding has also be seen at the low temperature [67]. The thermal energy activates the incommensurate states before reaching the equilibrium state. Wijn et al. theoretically examined the several physical parameters which affect the superlubric sliding on graphite surface [68]. They carried out Langevin simulations to observe the effect of thermal fluctuations on periodic orbits in the temperature range of 5–300 K. In another study, Bagchi et al. examine the rotational stability of tBLG with molecular dynamics simulation and found that the translational rotations of graphene flake in the temperature range of 300–3000 K are size-dependent [69]. They found that the number of potential energy barriers becomes higher as the flake dimension increases; therefore, the probability of rotation becomes negligible at high temperature. However, we believe that the incomplete periodicity of Moiré superlattices may be present in synthesized tBLG, which induces the periodic fluctuations in potential energy. These fluctuations are sufficient to induce the twisting between the layers. In addition to this, we assume that the sliding behavior of the graphene layer introduces the twisting as the temperature deviates from 300 K. The twisting between the layers takes place due to the strain generation from the substrate, and the contribution of the strain influences directly the degree of rotation. Furthermore, the twist angle has been assigned on the basis of peak parameters, which are obtained from temperature dependent Raman spectra in both the samples (tB_1 and tB_2).

Fig. 9 shows the twist angle variation with respect to temperature in the range of 80–450 K. In sample tB_1, the twist angle is estimated to be ~$23^\circ \leq \theta \leq 27^\circ$ and $3^\circ \leq \theta \leq 8^\circ$ for temperature below and above 300 K based on earlier twist angle assignment [20,25,48,49]. One can observe that the estimated twist angle is not close to the θc for the temperature range 80–450 K. These observations indicate that the tB_1 has a large twisting for $T \leq 300$ K and small twisting for $T > 300$ K. In sample tB_2, the twist angle has been

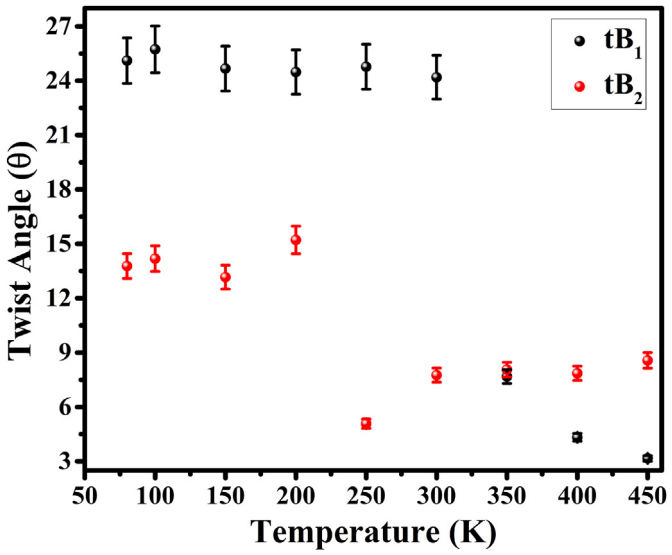

Fig. 9. The twist angle variation as a function of temperature in samples tB_1 and tB_2 from 80 to 450 K. The error bars represent the five percent of twist angle in each data point.

found ~13° ≤ θ ≤ 16° and 5° ≤ θ ≤ 9° for the temperature up to 200 K and 250– 450 K based on the earlier Raman studies [20,47]. In this case, the estimated twist angle is close to θc for T ≤ 200 K and a small angle regime for T ≥ 250 K. At last, the temperature variations on the Raman spectra in $tB_1$and tB_2 have been summarized in Table 2. The results point out that the temperature coefficient of the G peak is larger in tB_2 as compared to tB_1 and the tB_2 has a larger temperature coefficient of the 2D peak as compared to tB_1. The twist angle in tB_1 and tB_2 has a large angle regime below 300 and 250 K. In both samples, the twist angle has been found in a small angle regime at high temperatures. The appearance of a small twist angle at high temperature may be attributed to the torque generation, which varies with the derivative of the interlayer potential. The large sliding might be plausible cause of large twist angle at low temperature.

Nevertheless, the twist angle has been estimated based on Raman spectroscopy throughout this study. Still, the accurate determination of twist angle becomes complex at low and high temperatures due to the involvement of several factors, namely variation in laser power, the drift of laser spot, defects, graphene-substrate interaction, and doping. Thus, these interesting observations in twisted bilayer graphene reignite the need to further explore the unresolved factors during the twist angle determination, which could influence emerging graphene-derived quantum devices.

Table 2
Temperature coefficient ($\chi^{G,2D}$) and twist angle of samples tB_1 and tB_2 in the temperature range of 80–450 K.

Samples	Temperature Range	Temperature		Twist angle
	(K)	Coefficient (cm^{-1}/K)		(θ)
		G Peak		
tB_1	80–450	−0.0097	−0.0292	23°-27° (T ≤ 300 K) 3°-8°(T > 300 K)
tB_2	80–450	−0.0108	−0.0301	13°-16 °(80–200 K) 5°-9° (250–450 K)

4. Conclusion

In summary, we investigated the effect of temperature (80–450 K) on Raman scattering in two samples (tB_1 and tB_2) of twisted bilayer graphene (tBLG) film on Si/SiO_2 substrate. The twisting nature of bilayer graphene film has been confirmed based on R, G, and 2D peak properties in Raman spectra. The Raman mapping with respect to different peak parameters of G and 2D peak (intensity, width, and position), intensity ratio (I_{2D}/I_G) confirms the uniformity of the selected region of tBLG film. The R peak has been found at 1395.82 cm^{-1} in tB_1, and no R peak has been found in tB_2 at 300 K. The extracted value of the temperature coefficient of G peak has been found to be - (0.97 ± 0.34) × 10^{-2} cm^{-1}/K in tB_1 and -(1.08 ± 0.15) × 10^{-2} cm^{-1}/K in tB_2. The temperature coefficient of 2D peak has been found to be - (2.92 ± 0.80) × 10^{-2} cm^{-1}/K, and - (3.01 ± 0.29) × 10^{-2} cm^{-1}/K in tB_1, and tB_2. Additionally, the temperature variation on the twist angle has been studied based on the G and 2D peak in Raman spectra. In tB_1, the twist angle has been found to be ~23°-27°for T ≤ 300 K and 3°-8° for T > 300 K. In tB_2, the twist angle has been found to be ~13°-16° for the temperature range of 80–200 K and 5°-9° for 250–450 K. At high temperature, the twist angle lies within the scope of a small angle regime, which indicates the strong coupling between layers. At low temperature, the twist angle belongs to a large angle regime, which manifests the small interlayer interaction between layers. The obtained results highlight the importance of temperature variation on the twisting behavior of bilayer graphene film and its anharmonic properties.

CRediT authorship contribution statement

Girija Shankar Papanai: Conceptualization, Investigation, Methodology, Formal analysis, Writing – original draft. **Jasveer Singh:** Methodology, Software. **Nita Dilawar Sharma:** Validation, Writing – review & editing. **S.G. Ansari:** Methodology, Writing – review & editing. **Bipin Kumar Gupta:** Supervision, Conceptualization, Validation, Writing – review & editing.

Declaration of competing interest

The authors declare that they have no known competing financial interests or personal relationships that could have influenced the work reported in this paper.

Acknowledgments

Authors acknowledge the Director, CSIR-NPL, for providing the research facility for FTT mission mode project on the growth of graphene. The authors thank Mr. Amit Boora (OLYMPUS, Gurugram, India) and Dr. Sudhir Husale for their constant support in the Optical Microscopy facility. We are grateful to Ms. Neha Bura for the technical assistance and fruitful discussion regarding Raman spectroscopy measurements. G.S.P. acknowledges CSIR, India, for providing research fellowship. S G Ansari would like to acknowledge the measurement support received from the Central Instrumentation Facility and DST-PURSE program of Jamia Millia Islamia. We thank Dr. Shantanu Aggarwal (Application Scientist), Renishaw India, for the support.

Appendix A. Supplementary data

Supplementary data to this article can be found online at https://doi.org/10.1016/j.carbon.2021.02.083.

References

[1] H. Patel, L. Huang, C.-J. Kim, J. Park, M.W. Graham, Stacking angle-tunable photoluminescence from interlayer exciton states in twisted bilayer graphene, Nat. Commun. 10 (2019) 1445.

[2] U. Mogera, G.U. Kulkarni, A new twist in graphene research: twisted graphene, Carbon 156 (2020) 470–487.

[3] A. Kerelsky, L.J. McGilly, D.M. Kennes, L. Xian, M. Yankowitz, S. Chen, K. Watanabe, T. Taniguchi, J. Hone, C. Dean, A. Rubio, A.N. Pasupathy, Maximized electron interactions at the magic angle in twisted bilayer graphene, Nature 572 (2019) 95–100.

[4] A.H. MacDonald, R. Bistritzer, Graphene moiré mystery solved? Nature 474 (2011) 453–454.

[5] M. Yankowitz, S. Chen, H. Polshyn, Y. Zhang, K. Watanabe, T. Taniguchi, D. Graf, A.F. Young, C.R. Dean, Tuning superconductivity in twisted bilayer graphene, Science 363 (2019) 1059–1064.

[6] M.J. Park, Y. Kim, G.Y. Cho, S. Lee, Higher-order topological insulator in twisted bilayer graphene, Phys. Rev. Lett. 123 (2019) 216803.

[7] Y. Cao, V. Fatemi, S. Fang, K. Watanabe, T. Taniguchi, E. Kaxiras, P. Jarillo-Herrero, Unconventional superconductivity in magic-angle graphene superlattices, Nature 556 (2018) 43–50.

[8] A.L. Sharpe, E.J. Fox, A.W. Barnard, J. Finney, K. Watanabe, T. Taniguchi, M.A. Kastner, D. Goldhaber-Gordon, Emergent ferromagnetism near three-quarters filling in twisted bilayer graphene, Science 365 (2019) 605–608.

[9] Y. Cao, V. Fatemi, A. Demir, S. Fang, S.L. Tomarken, J.Y. Luo, J.D. Sanchez-Yamagishi, K. Watanabe, T. Taniguchi, E. Kaxiras, R.C. Ashoori, P. Jarillo-Herrero, Correlated insulator behaviour at half-filling in magic-angle graphene superlattices, Nature 556 (2018) 80–84.

[10] R. Bistritzer, A.H. MacDonald, Moiré butterflies in twisted bilayer graphene, Phys. Rev. B 84 (2011), 035440.

[11] T. Ohta, J.T. Robinson, P.J. Feibelman, A. Bostwick, E. Rotenberg, T.E. Beechem, Evidence for interlayer coupling and moiré periodic potentials in twisted bilayer graphene, Phys. Rev. Lett. 109 (2012) 186807.

[12] Z. Ni, L. Liu, Y. Wang, Z. Zheng, L.-J. Li, T. Yu, Z. Shen, G -band Raman double resonance in twisted bilayer graphene: evidence of band splitting and folding, Phys. Rev. B 80 (2009) 125404.

[13] G. Li, A. Luican, J.M.B. Lopes dos Santos, A.H. Castro Neto, A. Reina, J. Kong, E.Y. Andrei, Observation of Van Hove singularities in twisted graphene layers, Nat. Phys. 6 (2010) 109–113.

[14] G. Trambly de Laissardière, D. Mayou, L. Magaud, Localization of Dirac electrons in rotated graphene bilayers, Nano Lett. 10 (2010) 804–808.

[15] E. Suárez Morell, J.D. Correa, P. Vargas, M. Pacheco, Z. Barticevic, Flat bands in slightly twisted bilayer graphene: tight-binding calculations, Phys. Rev. B 82 (2010) 121407.

[16] J. Wang, X. Mu, L. Wang, M. Sun, Properties and applications of new superlattice: twisted bilayer graphene, Materials Today Physics 9 (2019) 100099.

[17] L. Brown, R. Hovden, P. Huang, M. Wojcik, D.A. Muller, J. Park, Twinning and twisting of tri- and bilayer graphene, Nano Lett. 12 (2012) 1609–1615.

[18] W.-T. Pong, C. Durkan, A review and outlook for an anomaly of scanning tunnelling microscopy (STM): superlattices on graphite, J. Phys. D Appl. Phys. 38 (2005) R329–R355.

[19] A.T. N'Diaye, J. Coraux, T.N. Plasa, C. Busse, T. Michely, Structure of epitaxial graphene on Ir(111), New J. Phys. 10 (2008), 043033.

[20] K. Kim, S. Coh, L.Z. Tan, W. Regan, J.M. Yuk, E. Chatterjee, M.F. Crommie, M.L. Cohen, S.G. Louie, A. Zettl, Raman spectroscopy study of rotated double-layer graphene: misorientation-angle dependence of electronic structure, Phys. Rev. Lett. 108 (2012) 246103.

[21] Y.-C. Chen, W.-H. Lin, W.-S. Tseng, C.-C. Chen, GeorgeR. Rossman, C.-D. Chen, Y.-S. Wu, N.-C. Yeh, Direct growth of mm-size twisted bilayer graphene by plasma-enhanced chemical vapor deposition, Carbon 156 (2020) 212–224.

[22] A. Jorio, L.G. Cançado, Raman spectroscopy of twisted bilayer graphene, Solid State Commun. 175–176 (2013) 3–12.

[23] Z.F. Wang, F. Liu, M.Y. Chou, Fractal landau-level spectra in twisted bilayer graphene, Nano Lett. 12 (2012) 3833–3838.

[24] A.C. Ferrari, D.M. Basko, Raman spectroscopy as a versatile tool for studying the properties of graphene, Nat. Nanotechnol. 8 (2013) 235–246.

[25] V. Carozo, C.M. Almeida, E.H.M. Ferreira, L.G. Cançado, C.A. Achete, A. Jorio, Raman signature of graphene superlattices, Nano Lett. 11 (2011) 4527–4534.

[26] R.W. Havener, H. Zhuang, L. Brown, R.G. Hennig, J. Park, Angle-resolved Raman imaging of interlayer rotations and interactions in twisted bilayer graphene, Nano Lett. 12 (2012) 3162–3167.

[27] A.A. Balandin, Phononics of graphene and related materials, ACS Nano 14 (2020) 5170–5178.

[28] H. Malekpour, A.A. Balandin, Raman-based technique for measuring thermal conductivity of graphene and related materials: thermal conductivity of graphene and related materials, J. Raman Spectrosc. 49 (2018) 106–120.

[29] J. Moser, A. Barreiro, A. Bachtold, Current-induced cleaning of graphene, Appl. Phys. Lett. 91 (2007) 163513.

[30] H. Li, H. Ying, X. Chen, D.L. Nika, A.I. Cocemasov, W. Cai, A.A. Balandin, S. Chen, Thermal conductivity of twisted bilayer graphene, Nanoscale 6 (2014) 13402–13408.

[31] I. Calizo, A.A. Balandin, W. Bao, F. Miao, C.N. Lau, Temperature dependence of the Raman spectra of graphene and graphene multilayers, Nano Lett. 7 (2007) 2645–2649.

[32] H. Zhou, C. Qiu, F. Yu, H. Yang, M. Chen, L. Hu, Y. Guo, L. Sun, Raman scattering of monolayer graphene: the temperature and oxygen doping effects, J. Phys. D Appl. Phys. 44 (2011) 185404.

[33] W. Wang, Q. Peng, Y. Dai, Z. Qian, S. Liu, Temperature dependence of Raman spectra of graphene on copper foil substrate, J. Mater. Sci. Mater. Electron. 27 (2016) 3888–3893.

[34] P.K. Kashyap, I. Sharma, B.K. Gupta, Continuous growth of highly reproducible single-layer graphene deposition on Cu foil by indigenously developed LPCVD setup, ACS Omega 4 (2019) 2893–2901.

[35] X. Liang, B.A. Sperling, I. Calizo, G. Cheng, C.A. Hacker, Q. Zhang, Y. Obeng, K. Yan, H. Peng, Q. Li, X. Zhu, H. Yuan, A.R. Hight Walker, Z. Liu, L. Peng, C.A. Richter, Toward clean and crackless transfer of graphene, ACS Nano 5 (2011) 9144–9153.

[36] P.Y. Huang, C.S. Ruiz-Vargas, A.M. van der Zande, W.S. Whitney, M.P. Levendorf, J.W. Kevek, S. Garg, J.S. Alden, C.J. Hustedt, Y. Zhu, J. Park, P.L. McEuen, D.A. Muller, Grains and grain boundaries in single-layer graphene atomic patchwork quilts, Nature 469 (2011) 389–392.

[37] A.C. Ferrari, Raman spectroscopy of graphene and graphite: disorder, electron–phonon coupling, doping and nonadiabatic effects, Solid State Commun. 143 (2007) 47–57.

[38] L.M. Malard, M.A. Pimenta, G. Dresselhaus, M.S. Dresselhaus, Raman spectroscopy in graphene, Phys. Rep. 473 (2009) 51–87.

[39] R. Saito, A. Grüneis, G.G. Samsonidze, V.W. Brar, G. Dresselhaus, M.S. Dresselhaus, A. Jorio, L.G. Cançado, C. Fantini, M.A. Pimenta, A.G.S. Filho, Double resonance Raman spectroscopy of single-wall carbon nanotubes, New J. Phys. 5 (2003) 157, 157.

[40] L. Liu, H. Zhou, R. Cheng, W.J. Yu, Y. Liu, Y. Chen, J. Shaw, X. Zhong, Y. Huang, X. Duan, High-yield chemical vapor deposition growth of high-quality large-area AB-stacked bilayer graphene, ACS Nano 6 (2012) 8241–8249.

[41] Z. Yan, Z. Peng, Z. Sun, J. Yao, Y. Zhu, Z. Liu, P.M. Ajayan, J.M. Tour, Growth of bilayer graphene on insulating substrates, ACS Nano 5 (2011) 8187–8192.

[42] A.I. Cocemasov, D.L. Nika, A.A. Balandin, Phonons in twisted bilayer graphene, Phys. Rev. B 88 (2013), 035428.

[43] C.H. Lui, L.M. Malard, S. Kim, G. Lantz, F.E. Laverge, R. Saito, T.F. Heinz, Observation of layer-breathing mode vibrations in few-layer graphene through combination Raman scattering, Nano Lett. 12 (2012) 5539–5544.

[44] F. Herziger, P. May, J. Maultzsch, Layer-number determination in graphene by out-of-plane phonons, Phys. Rev. B 85 (2012) 235447.

[45] C.-C. Lu, Y.-C. Lin, Z. Liu, C.-H. Yeh, K. Suenaga, P.-W. Chiu, Twisting bilayer graphene superlattices, ACS Nano 7 (2013) 2587–2594.

[46] J. Campos-Delgado, L.G. Cançado, C.A. Achete, A. Jorio, J.-P. Raskin, Raman scattering study of the phonon dispersion in twisted bilayer graphene, Nano Res 6 (2013) 269–274.

[47] S. Coh, L.Z. Tan, S.G. Louie, M.L. Cohen, Theory of the Raman spectrum of rotated double-layer graphene, Phys. Rev. B 88 (2013) 165431.

[48] V. Carozo, C.M. Almeida, B. Fragneaud, P.M. Bedê, M.V.O. Moutinho, J. Ribeiro-Soares, N.F. Andrade, A.G. Souza Filho, M.J.S. Matos, B. Wang, M. Terrones, R.B. Capaz, A. Jorio, C.A. Achete, L.G. Cançado, Resonance effects on the Raman spectra of graphene superlattices, Phys. Rev. B 88 (2013), 085401.

[49] Y. Wang, Z. Su, W. Wu, S. Nie, N. Xie, H. Gong, Y. Guo, J. Hwan Lee, S. Xing, X. Lu, H. Wang, X. Lu, K. McCarty, S. Pei, F. Robles-Hernandez, V.G. Hadjiev, J. Bao, Resonance Raman spectroscopy of G-line and folded phonons in twisted bilayer graphene with large rotation angles, Appl. Phys. Lett. 103 (2013) 123101.

[50] R. He, T.-F. Chung, C. Delaney, C. Keiser, L.A. Jauregui, P.M. Shand, C.C. Chancey, Y. Wang, J. Bao, Y.P. Chen, Observation of low energy Raman modes in twisted bilayer graphene, Nano Lett. 13 (2013) 3594–3601.

[51] P. Tan, Y. Deng, Q. Zhao, W. Cheng, The intrinsic temperature effect of the Raman spectra of graphite, Appl. Phys. Lett. 74 (1999) 1818–1820.

[52] D. Yoon, Y.-W. Son, H. Cheong, Negative thermal expansion coefficient of graphene measured by Raman spectroscopy, Nano Lett. 11 (2011) 3227–3231.

[53] J.S. Park, A. Reina, R. Saito, J. Kong, G. Dresselhaus, M.S. Dresselhaus, G′ band Raman spectra of single, double and triple layer graphene, Carbon 47 (2009) 1303–1310.

[54] M.A. Pimenta, G. Dresselhaus, M.S. Dresselhaus, L.G. Cançado, A. Jorio, R. Saito, Studying disorder in graphite-based systems by Raman spectroscopy, Phys. Chem. Chem. Phys. 9 (2007) 1276–1290.

[55] A. Eckmann, A. Felten, A. Mishchenko, L. Britnell, R. Krupke, K.S. Novoselov, C. Casiraghi, Probing the nature of defects in graphene by Raman spectroscopy, Nano Lett. 12 (2012) 3925–3930.

[56] A.I. Cocemasov, D.L. Nika, A.A. Balandin, Engineering of the thermodynamic properties of bilayer graphene by atomic plane rotations: the role of the out-of-plane phonons, Nanoscale 7 (2015) 12851–12859.

[57] D.L. Nika, A.I. Cocemasov, A.A. Balandin, Specific heat of twisted bilayer graphene: engineering phonons by atomic plane rotations, Appl. Phys. Lett. 105 (2014), 031904.

[58] T. Shimada, T. Sugai, C. Fantini, M. Souza, L.G. Cançado, A. Jorio, M.A. Pimenta, R. Saito, A. Grüneis, G. Dresselhaus, M.S. Dresselhaus, Y. Ohno, T. Mizutani, H. Shinohara, Origin of the 2450 cm^{-1} Raman bands in Hopg, single-wall and double-wall carbon nanotubes, Carbon 43 (2005) 1049–1054.

[59] T.M.G. Mohiuddin, A. Lombardo, R.R. Nair, A. Bonetti, G. Savini, R. Jalil, N. Bonini, D.M. Basko, C. Galiotis, N. Marzari, K.S. Novoselov, A.K. Geim, A.C. Ferrari, Uniaxial strain in graphene by Raman spectroscopy: G peak splitting, Grüneisen parameters, and sample orientation, Phys. Rev. B 79 (2009) 205433.

[60] Z.H. Ni, T. Yu, Y.H. Lu, Y.Y. Wang, Y.P. Feng, Z.X. Shen, Uniaxial strain on graphene: Raman spectroscopy study and band-gap opening, ACS Nano 2 (2008) 2301–2305.
[61] N. Kim, K.S. Kim, N. Jung, L. Brus, P. Kim, Synthesis and electrical characterization of magnetic bilayer graphene intercalate, Nano Lett. 11 (2011) 860–865.
[62] S.S. Lin, B.G. Chen, C.T. Pan, S. Hu, P. Tian, L.M. Tong, Unintentional doping induced splitting of G peak in bilayer graphene, Appl. Phys. Lett. 99 (2011) 233110.
[63] I. Calizo, S. Ghosh, W. Bao, F. Miao, C. Ning Lau, A.A. Balandin, Raman nanometrology of graphene: temperature and substrate effects, Solid State Commun. 149 (2009) 1132–1135.
[64] A. Forestier, F. Balima, C. Bousige, G. de S. Pinheiro, R. Fulcrand, M. Kalbáč, D. Machon, A. San-Miguel, Strain and piezo-doping mismatch between graphene layers, J. Phys. Chem. C 124 (2020) 11193–11199.
[65] K.M. Omambac, H. Hattab, C. Brand, G. Jnawali, A.T. N'Diaye, J. Coraux, R. van Gastel, B. Poelsema, T. Michely, F.-J. Meyer zu Heringdorf, M.H. Hoegen, Temperature-controlled rotational epitaxy of graphene, Nano Lett. 19 (2019) 4594–4600.
[66] A.M. Popov, I.V. Lebedeva, A.A. Knizhnik, Y.E. Lozovik, B.V. Potapkin, Commensurate-incommensurate phase transition in bilayer graphene, Phys. Rev. B 84 (2011), 045404.
[67] X. Feng, S. Kwon, J.Y. Park, M. Salmeron, Superlubric sliding of graphene nanoflakes on graphene, ACS Nano 7 (2013) 1718–1724.
[68] A.S. de Wijn, C. Fusco, A. Fasolino, Stability of superlubric sliding on graphite, Phys. Rev. E. 81 (2010), 046105.
[69] S. Bagchi, H.T. Johnson, H.B. Chew, Rotational stability of twisted bilayer graphene, Phys. Rev. B 101 (2020), 054109.